

## Preface

## Introduction to special issue on geologic remote sensing



## A B S T R A C T

Herein we provide an overview of science and technology involved in remote sensing, and outlines some practical constraints in applications to geological problems. We further summarize diagnostic spectral features of important geological material that can be detected using satellite- and air-borne remote sensing. Finally, the papers contained in the special issue are briefly introduced.

## 1. Introduction

Remote sensing involves remote measurement of electromagnetic radiation reflected or emitted by Earth's surface using space-borne, air-borne and ground-based sensors. More formally, remote sensing involves the measurement of *solar electromagnetic radiance reflected* or *electromagnetic radiance emitted* by Earth's surficial material in a given wave length band and is measured in the units of  $\text{Watts}/\text{m}^{-2}/\text{sr}^{-1}$ . Most modern remote sensing instruments employ electro-optical sensors comprising photon detectors (charged coupled devices, CCDs) that convert the incoming radiance to electrical signal, and use predetermined transformation functions to transform the analogue electrical signal to discrete digital numbers. These digital numbers are imaged, georegistered and distributed in form of remote sensing images.

Although the remote sensing technology evolved over a period of more than a thousand years, the modern satellite-based remote sensing systems evolved directly from early orbital missions to photograph inner planets including Earth, Mars, Venus and the moon from the space. Geologic remote sensing of Earth can be considered to initiate in 1972 with the launch of ERTS-1 (the first Earth Resources Technology Satellite), later renamed as LANDSAT 1, by NASA. LANDSAT 1 marked the beginning of the LANDSAT series, which is the longest satellite data record of Earth's land surface, culminating in the currently operational LANDSAT 8. LANDSAT 1 was followed by several remote sensing programmes by various countries. From the point of view of geological remote sensing, two outstanding and widely used satellite-borne instruments are the multispectral Advanced Space-borne Thermal Emittance and Reflection Radiometer (ASTER; Abrams, 2000, Yamaguchi et al., 1998, Abrams and Hook, 1995) on-board Terra and hyperspectral Hyperion on-board EO-1 (Pearlman et al., 2003).

Depending on whether the reflected or emitted radiation is measured, a remote sensing system is classified into optical remote sensing system or emittance remote sensing system (Colwell, 1983). The former type measures the solar electromagnetic radiance reflected by Earth's surficial material, while the latter type measures the electromagnetic radiance emitted by Earth's surface. Every geologic material has unique reflectance and emittance (see next section), and therefore, in principle, it should be possible to characterize all surficial geologic materials by

optical or emittance remote sensing (Hunt, 1977; Clark, 1999; Cooper et al., 2002). However, in practice this is not possible because of two reasons.

First and foremost, the amount of energy available for reflectance and emittance remote sensing varies with wavelength, and hence it is not possible to derive continuous reflectance or emittance spectra from gamma ray wavelengths to radio waves. As a result, in practice, it is possible to characterize only those geologic materials through remote sensing that show diagnostic spectral features in the wavelengths for which there is sufficient energy available. According to the Plank's Equation for black body radiation, these wavelengths are 0.3–2.5  $\mu\text{m}$  (that is near Ultraviolet – Visible – Near Infrared – Short Wave Infrared or UV-VNIR-SWIR region of the electromagnetic spectrum) for optical remote sensing and 3 to 14  $\mu\text{m}$  (that is, thermal infrared or TIR region of the electromagnetic spectrum) for thermal emittance (or TIR) remote sensing.

Secondly, not all electromagnetic radiation within the UV-VNIR-SWIR and TIR regions listed above are transmitted by the atmosphere (Elachi and Zyl, 2006). Atmospheric gases such as water vapor, ozone, carbon dioxide, methane, oxygen and nitrous oxide absorb many of the wavelengths within the above region, and therefore the atmosphere becomes opaque with respect to radiation corresponding to these wavelengths (Fig. 1, Elachi and Zyl, 2006). As a result, there are very few atmospheric windows available for remote sensing. Satellite- borne and air-borne remote sensing is used to characterize and map only those geologic materials that show diagnostic spectral features within the above atmospheric windows.

## 2. Origin of spectral features of geologic materials

## 2.1. Visible-Near Infrared-Shortwave infrared region

Spectral features in a reflectance spectrum over the VNIR-SWIR Region record the interaction of the surface of a solid material with the incident electromagnetic energy. In the context of geologic remote sensing, the main interaction mechanisms are (1) electronic excitations and (2) vibrational excitations, which lead to transitions in the electronic and molecular vibration energy levels, respectively (Gaffey et al., 1997; Elachi and Zyl, 2006). Because all energy levels in nature are

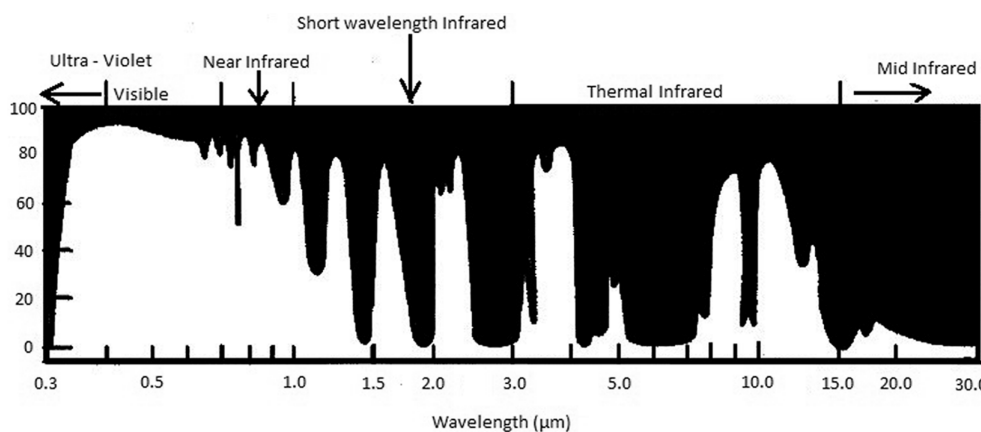


**Fig. 1.** Atmospheric windows for remote sensing (Modified after Elachi and Zyl, 2006).

quantized, each transition to a higher energy level involves absorption of specific quantum of energy (or, energy of specific wavelength) that is characteristic of the electronic and molecular configuration of the material. As a result, every geologic material has a unique set of absorption features depending on its chemical composition, and/or molecular and crystal structure.

Transitions in electronic energy states typically involve high energy and, therefore, the spectral absorption features caused by the changes in the electronic energy states appear in the VNIR-SWIR region. The main mechanisms involving electronic transition are (Burns, 1997): (1) crystal field transitions of electrons, that is, transitions of electrons between non-degenerate d orbitals in transition metal (mainly, Fe) bearing silicate minerals, (2) metal-to-metal or intervalence charge transfer (IVCT transitions) between adjacent cations in the silicate crystal structure, and (3) oxygen-to-metal charge transfer (OMCT transitions) in the silicate crystal structure. The most important electronic transition mechanism in geologic materials is crystal field splitting, which refers to the loss of degeneracy of the five d-orbitals of transition metals in the presence of a legend field in a coordination compound (Burns, 1970). Silicate minerals are essentially coordination compounds comprising exceedingly strong complex ions, the silicate anions ( $\text{SiO}_4^{4-}$ ), held together by a variety of metal cations ranging from transition metal cations (mainly  $\text{Fe}^{+2}$ ) to alkaline earth metals cations (mainly  $\text{Mg}^{+2}$ ,  $\text{Ca}^{+2}$ ) and alkali metals cations (mainly  $\text{Na}^+$ ,  $\text{K}^+$ ). However, crystal field splitting can occur only in  $\text{Fe}^{+2}$  bearing silicate minerals, and therefore, only the mafic silicate minerals such as olivine, pyroxene and amphiboles show absorption features caused by crystal field splitting. The crystal field splitting energy depends on the coordination geometry and the ionic radius and charge of the central metal cation. As a result, the substitution of  $\text{Fe}^{+2}$  by smaller cations such as  $\text{Mg}^{+2}$  results in a more compact coordination geometry and hence higher crystal field splitting energy, while the substitution of  $\text{Fe}^{+2}$  by larger cations such as  $\text{Ca}^{+2}$  results in a less compact coordination geometry and hence lower crystal field splitting energy (Burns, 1997; Gaffey et al., 1997). These substitutions cause, respectively, blue shift and red shift in the corresponding absorption features (Burns, 1997). Felsic silicates do not contain transition metals and therefore are not easily detected from optical remote sensing.

All molecules at temperatures above the absolute zero are in a state of perpetual motion. These motions are of two types (Gaffey et al., 1997): (1) internal vibrational motions which are characterized by changes in the lengths and angles of the bonds between the constituent atoms; and (2) external translational and rotational motions in which the molecule as a whole translates and rotates along the x, y and z axes. The vibrational, translational and rotational energies associated with each of these modes of motion is unique for every molecule depending on its chemical composition and bond geometry and, like all energies in nature, quantized. Any incident electromagnetic energy causes the

molecule to absorb specific amount of energy and transit to higher energy levels, giving rise to absorption features in reflectance spectra. The translational and rotational energy transitions require smaller energy, and hence the absorption features caused by these transitions appear in Far Infrared and Microwave region. However, the transitions in the vibrational energy levels of most molecules found in geologic materials correspond to VNIR-SWIR and TIR regions. The first excited vibrational energy level is called fundamental, and subsequent levels are called overtones. The fundamental energy states for most molecular vibrations generally occur in TIR and MIR (Mid Infrared) region; however, their overtones can occur in SWIR and VNIR region (Gaffey et al., 1997).

## 2.2. Thermal infrared region

The property of interest for remote compositional mapping of geologic materials in the TIR region is thermal emissivity, a wavelength specific quantity that is defined as the ratio of the radiance emitted by the body to the radiance emitted by an ideal black body at the same temperature (Hapke, 1993). The latter is estimated from the Plank's Equation for black body radiation. The emissivity of a body varies with wavelength, and an emissivity spectrum shows the variation of emissivity with wavelength. According to the Kirchoff's Law, emissivity of a given body at a given wavelength is equal to its absorptance at the same wavelength, and therefore an emissivity spectrum can also be considered to indirectly record the interaction of a body with the electromagnetic radiation. In particular, strong absorption bands are associated with high reflectance because of the Reststrahlen Effect (Salisbury, 1997; Elachi and Zyl, 2006), and therefore coincide with minima in emissivity spectra. In the case of silicate minerals, spectral absorption features due to transition of the vibrational energy of the Si-O asymmetric stretching to the fundamental occur between 8 and 12  $\mu\text{m}$  (Kahle et al., 1997; Salisbury, 1997). Typically, the Si-O fundamental absorption features shift to shorter wavelengths as the bond strength within the crystal lattice increases because of increasing polymerization of the silica tetrahedra (Vincent and Thomson, 1972; Hunt and Salisbury, 1974). Thus, the Si-O fundamental absorption features and the corresponding Reststrahlen minima in emissivity spectra display a blue shift from 11.5  $\mu\text{m}$  in the case of nesosilicates to 9  $\mu\text{m}$  in the case of tectosilicates (Vickers and Lyon, 1967; Hunt and Salisbury, 1974; Hunt, 1980). Because 8 and 12  $\mu\text{m}$  falls with the TIR atmospheric window, the emissivity spectra obtained from TIR remote sensing can be used to remotely map both felsic and mafic silicates.

## 3. Geologic remote sensing: Practical limitations

A large body of literature is available on geological applications of remote sensing, including remote mapping of geological material from

**Table 1**

Diagnostic spectral features of minerals that can be detected using multispectral and hyperspectral remote sensing.

Mineral Family	Mineral	NIR – SWIR Range		TIR Range	
		Diagnostic Feature ( $\mu\text{m}$ )	Attribution	Diagnostic Feature ( $\mu\text{m}$ )	Attribution
Olivine	Forsterite	~1.04	Crystal Field Effects (CFE)	~10.00 ~10.98 ~11.76	Fundamental vibration (Si – O stretching)
	Fayalite	~1.08	CFE	~10.50 ~12.10	Fundamental vibration (Si – O stretching)
Pyroxene	Bronzite	~0.90 ~1.85	CFE		
	Ferrosilite	~1.17	CFE		
	Pigeonite	0.8–0.95 1.90–2.20	CFE (Distorted Octahedra)		
	Augite	0.70–0.80 2.10–2.30	Charge Transfer (Fe <sup>+2</sup> –Fe <sup>+3</sup> ) Crystal Field Effects (CFE)	~10.00, ~10.52 ~14.28	Fundamental vibration (Si – O stretching)
	Diopside	~0.85 ~1.05 ~2.30	Charge Transfer (Fe <sup>+2</sup> –Fe <sup>+3</sup> ) CFE	~10.00 ~10.52–11.00 ~14.28	Fundamental vibration (Si – O stretching)
	Hedenbergite	~0.98 ~1.18 ~1.03 ~2.03	CFE (Fe at M1 Site) Weak CFE (Fe at M2 Site) Intense	~8.70 ~10.00 ~10.52–11.00 ~14.28	Fundamental vibration (Si – O stretching)
Amphibole	Orthopyroxene	0.90–0.94 1.85–2.04	CFE (Fe at M1 Site) CFE (Fe at M2 Site)		
	Hornblende	~0.65 ~1.45 2.25–2.35 ~1.00, 2.30	Charge Transfer (Fe) Vibrational (OH) Vibrational (Fe-OH) CFE (Fe <sup>+2</sup> )	~8.50 ~12.25	Fundamental vibration (Si – O stretching)
Mica	Biotite	~1.10 2.30–2.40	CFE (Fe <sup>+2</sup> ) Vibrational (Mg-OH) Doublet		
	Muscovite	~1.40 ~2.80 2.25–2.40	Vibrational (OH) Vibrational (Al-OH) Triplet	~10.00, ~13.30	Fundamental vibration (Si – O stretching)
Clays	Illite	~0.80 ~1.20 ~1.40 ~2.80 and ~1.90 2.25–2.40	Charge Transfer or CFE (Fe + 2) Vibrational (OH) and (H <sub>2</sub> O) Vibrational (Al-OH) Triplet		
	Gibbsite	~1.55 2.30–2.50	Vibrational (OH) Vibrational (Al-OH)		
	Kaolinite	~1.50 ~1.90 2.30–2.40	Vibrational (OH), (H <sub>2</sub> O) Weak Vibrational (Al-OH) Triplet	~10.00 ~10.96 ~14.5	Fundamental vibration (Si – O stretching)
	Dickite	~1.45 2.30–2.40	Vibrational (OH) Intense Vibrational (Al-OH) Triplet	~9.09, ~10.00, ~10.50, ~12.50	Fundamental vibration (Si – O stretching)
	Lizardite	~1.45 2.00–2.20, 2.30–2.50	Vibrational (OH) Vibrational (Mg-OH)	~9.00–11.50, ~14.25	Fundamental vibration (Si – O stretching)
	Pyrophyllite	~1.40 2.10–2.40	Vibrational (OH) Narrow & Sharp Vibrational (Al-OH) Triplet	~9.50–11.50, ~12.50	Fundamental vibration (Si – O stretching)
	Montmorillonite	~1.45, ~1.90 2.10–2.30	Vibrational (OH) & (H <sub>2</sub> O) Vibrational (Al-OH) Triplet	~9.00, ~12.50	Fundamental vibration (Si – O stretching)
	Nontronite	~1.0 ~1.45, ~1.90 2.20–2.40	CFE (Fe <sup>3+</sup> ) Vibrational (OH) & (H <sub>2</sub> O) Vibrational (Al-OH) Triplet	~10.00, ~12.50	Fundamental vibration (Si – O stretching)

(continued on next page)

**Table 1** (continued)

Mineral Family	Mineral	NIR – SWIR Range		TIR Range	
		Diagnostic Feature (μm)	Attribution	Diagnostic Feature (μm)	Attribution
Others	Hematite	~0.885 ~0.64	Laporte-forbidden transitions	~9.50 ~11.00 ~14.00	
	Magnetite	~0.20–2.0 (except ~0.8)	Causes are not agreed upon for very low reflectance	~8.3 ~10.00 ~14.00	
	Ilmenite	~0.50 and 1.23	CFE of Ti <sup>3+</sup> or to (Fe <sup>2+</sup> -Ti <sup>3+</sup> )		
	Calcite	~2.00 and ~2.30	Vibrational (CO <sub>3</sub> ) Intense Triad	~10.00 ~11.50 ~14.00	Fundamental Vibration (CO <sub>3</sub> )
	Dolomite	~2.00 and ~2.30	Vibrational (CO <sub>3</sub> ) Weak at 1.9	~8.50, ~11.50, ~13.50	Fundamental Vibration (CO <sub>3</sub> )
	Gypsum	~1.50 and ~1.90	Vibrational (H <sub>2</sub> O) Intense	~8.00 9.00–10.00	Fundamental vibration (S – O)
	Quartz	–	No Diagnostic Features	(~7.50, ~8.50) (~12.00, ~12.5)	Fundamental vibration (Si – O stretching)
	Syenite	2.5–3.5	Vibrational (H <sub>2</sub> O & OH)	~8.00 ~0.90	Fundamental vibration (Si – O stretching)

Sources: Gaffey et al. (1997); spectral libraries compiled by Clark, 1999 and Lafuente et al. (2015).

satellite-borne remote sensing images. The major application areas are surface lithological and regolith mapping (Fraser et al., 1997; Schetselaar et al., 2000; Rowan and Mars, 2003; Hewson et al., 2005; Gomez et al., 2005; Watts et al., 2005; Vaughan et al., 2005; Gad and Kusky, 2006; Li et al., 2007; Khan et al., 2007; Rockwell and Hofstra, 2008; Qari et al., 2008; Massironi et al., 2008); hydrothermal alteration mapping (Kruse et al., 1990; Crosta et al., 1998; Rowan et al., 2000; Hubbard et al., 2003; Yamaguchi and Naito, 2003; Kavak, 2005; Vaughan et al., 2005; van der Meer, 2006; Kruse et al., 2006; Mars and Rowan, 2006, 2010, 2011; Zhang et al., 2007; Chen et al., 2007; Gersman et al., 2008; Carranza et al., 2008; Bedini et al., 2009; Madani and Emam, 2011; Oztan and Suzen, 2011), structural mapping (Yesou et al., 1993; Boccaletti et al., 1998); detection of hydrocarbon seeps (Macdonald et al., 1993; van der Meer et al., 2002); and geothermal energy systems (Vaughan et al., 2005; Yang et al., 2000, 2001; Kratt et al., 2010; Hellman and Ramsey, 2004). Hydrated and hydrothermal minerals have also been mapped on the Martian surface using orbital remote sensing data (Wang et al., 2006; Aubrey et al., 2006; Loizeau et al., 2007; Mangold et al., 2008; Mustard et al., 2008; Ehlmann et al., 2009; Bishop et al., 2016; Singh et al., 2017 (this issue)). In the past two decades, hyperspectral data which are characterized by large numbers of narrow (~10 nm), contiguous bands and, therefore, provide continuous spectra over the entire VNIR-SWIR range, have become widely available. Air-borne and space-borne hyperspectral sensors, most of which are commercial, have been widely used for geological mapping and exploration targeting, and have proved to be highly effective (Goetz et al., 1985; Goetz and Kindel, 1996; Cudahy et al., 2002; Kruse et al., 1993, 1999, 2003; Kruse, 1988, 2008, 2012, 2015; Van der Meer et al., 2012).

However, notwithstanding the strong theoretical basis outlined in Section 2 above and numerous successful case studies, geologic remote sensing has several limitations in practice:

- (1) Short wavelength electromagnetic radiation has no penetration and therefore optical remote sensing gives information about only the surface, which is a severe limitation in the areas with low outcrop density. In case of in-situ regolith, the composition of regolith can be used to gain insights into the composition of underlying rocks, but transported regolith or soil cover or wind-blown sand cover can completely hide the geology; and
- (2) Even in the case of outcropping area, spectral mixing is a major problem. Geologic material typically is a heterogeneous mixture of

a variety of minerals, and the mixing is microscopic. As a result, the incident solar radiation is reflected multiple times by different constituents of the geologic material before it is directed to the satellite-borne or air-borne sensor. The radiance that is received at the sensor is therefore the integrated response of multiple minerals. The inversion of the radiance received at the sensor to obtain the response of the individual minerals is non-trivial, and no good unmixing models are available for geological material. The spectral mixing problem is further compounded by limitations in spatial resolutions of remote sensing images – the larger the pixel size, the higher the spectral mixing. If, in order to decrease spectral mixing, the spatial resolution is increased by reducing the instantaneous field of view (IFOV) of the sensor as in the case of multispectral sensors, the spectral resolution is compromised to maintain good signal to noise ratio. At low spectral resolutions of wide band multispectral images such as LANDSAT and ASTER, it is difficult to resolve the narrow diagnostic absorption features of geological material, and compositional mapping cannot be efficiently carried out.

However, notwithstanding the limitations, a large number of minerals can be remotely detected using the existing multispectral and hyperspectral sensors. Table 1 summarizes the spectral features of minerals that can be detected with high degree of confidence from open file available remote sensing data.

#### 4. The way forward

The biggest advantage of remote sensing data is synoptic and unbiased coverage of large areas. However, it is important to realize that these data provide information only about the spectral and thermal properties of the top few millimeters of the Earth's surface. In the field of mineral exploration in areas of cover such as Australia, large parts of India, China and West Africa, and in order to make optimal utilization of remote sensing data, it is important to integrate the spectral data with the geological context provided by the surface geochemistry, geophysics, reolith, basement structures, geology, sedimentary systems and landscape evolution (e.g., Anand and Butt, 2010; Anand 2015; Butt, 2016; González-Álvarez et al., 2016; Lampinen et al., 2017). This integration provides the framework and a more geological meaningful interpretation to the remote sensing data interpretations.

The protocol to use remote sensing datasets should be established

and include ground cross-reference, not just at the end of the exercise but in three phases: (1) preliminary assessment to establish what there is for observation and the best technique to apply for this; (2) CA/CQ tuning of the preliminary results by ground-truthing to tune the approach and constraining the interpretations by the parameters imposed by geological context (or any other context type) where the technique is applied; and (3) ground-truthing of the final assessment. Each remote sensing interpretation should have an assessment on uncertainty of the observation, data processing and interpreted results.

In terms of technology, there is surge of interest in UAV-based hyperspectral and ultraspectral remote sensing. Because of lower flying heights, it is possible to obtain high spectral and spatial resolution images from these sensors without compromising on signal to noise ratios (Colomina and Molina, 2014; Pajares, 2015). Although the technology is nascent and the images require significant corrections before they can be interpreted, algorithms are being developed for corrections and interpretations of these images (Turner et al., 2014; Aasen et al., 2015; Conte et al., 2018; Tayara et al., 2018; Sledz et al., 2018). UAV-based remote sensing can potentially revolutionize geographic remote sensing in the next decade.

## 5. Summary of research papers in the special issue

This Special Issue of Ore Geology Reviews on Geologic Remote Sensing contains 9 papers on a variety of geological applications of remote sensing.

**Shevyrev (2018)** (this issue) uses in-situ observations with geological mapping data, Landsat 8 images and SRTM DEMs to study the tectonic deformation and ore controlling structures associated with the Mnogovershinnoe epithermal gold-silver deposit and the related multiphase Paleogene Bekchiul granitoid pluton located in the northern part of the East Sikhote-Alin magmatic belt, North-East Russia. The author also analysed isostatic upliftment and erosion levels in streams in the study area using base level modelling to identify local uplifts that are associated with the core part of the Bekchiul massif and also with gold placers. Infusing all information and data, the author reconstructed the neotectonics of the Bekchiul volcanic-plutonic center and the evolution of its relief and tectonic structures since the Upper Cretaceous. He further used isotopic dating of Neogene-Quaternary processes to conclude that the Mesozoic tectonic activity continued into the Cenozoic.

**Vasuki et al. (2018)** (this issue) apply machine learning algorithms to Landsat time series data to study spatial and temporal changes in land cover associated with clearing, excavation and rehabilitation activities related to bauxite mining in the Darling Range in Western Australia. The authors used support vector machine, random forest and Naïve Bayes machine learning algorithms, among which Random forest achieved the highest accuracy of 95%. The results were validated using the records of rehabilitation and land clearing kept by the mining companies. A close correlation was observed between the automated analysis outputs and the company's records. Their paper demonstrates the potential use of machine analysis in improving the accuracy of spatial data related to land clearing; and in monitoring vegetation recovery of closed and rehabilitated mines.

**Sankaran et al. (this issue)** review published literature on applications of ASTER data for mapping various types of mineralized zones and industrial rocks in the Sultanate of Oman, which is characterized by arid desertic terrains. The authors summarise and review various image processing techniques and spectral indices that have been used for demarcation of chromite, manganese, Ni-magnesioferrite–magnetite–awaruite and volcanic massive sulfide (VMS) deposits and as well as industrial rocks such as limestone, dolomite, clay and marble in the Sultanate of Oman. These techniques can be used to identify similar deposits in arid regions across the world.

**Ninomiya and Fu (2018)** (this issue) review geologic applications of thermal infrared data collected by ASTER and other thermal infrared sensors. They discuss the spectroscopic basis of analyzing and

interpreting the multispectral thermal infrared remote sensing data, and include a review of the historical studies, methodology of spectral measurements and comparison of laboratory/field spectra with those measured remotely. They further review previous studies on lithological and mineralogical napping using TIR multispectral remote sensing data. A major highlight of the paper is a summary of spectral indices for extracting information on the mineralogy and chemistry of geological materials.

**Kumar et al. (2018)** (this issue) propose a novel method of spectral mapping of phosphate deposits in dolomitic and carbonatic rocks by applying reflectance spectroscopy and ASTER data processing. The study exercise delineates dolomite-hosted rock phosphate around Udaipur City, Western India. The images were enhanced by ACE and MF methods applied to ASTER SWIR bands and delineated rock-phosphate-rich zones within the carbonates rock suites. The results were ground-truth in the field by a qualitative colorimetric method and comparing image spectra of anomalous zones with the ASTER laboratory spectra of rock phosphate samples. The authors present a solid methodology applicable to mineral exploration of phosphate-rich rocks in similar geological contexts in different continents.

**Zhao et al. (2018)** (this issue) discuss the applicability of Landsat Operational Land Imager data to identify rock outcrops in a covered-dominated terrain of loess (97% cover) in the northern Baoji district, China. The authors focussed on the interpretation of strata, fractures and lineaments. The methodology applied was to clip the area of interest using slope and topographical analysis, the band ratio (B4/B2), fractal summation algorithms, spatial clumping and hot-spot analysis to filter for false anomalies. In parallel, high-resolution Worldview 2 data was used for visual direct interpretation. The authors report a new criterion to identify rocky outcrops in the Baoji district which is not based on spectral features but spatial clustering. This research has special application and impact in the mineral exploration undercover space.

**Singh et al. (2017)** (this issue) present a comprehensive review on impact-related hydrothermal activity in Martian craters by the identification of hydrous and hydrated minerals. The datasets used to detect and map these mineralogies are orbital imaging spectroscopic and high-resolution panchromatic and digital elevation data. The detection span from phyllosilicates such as smectites, kaolinites, prehnites, chlorites, and mica, to tectosilicates (hydrated silica). The authors interpreted the presence of reported chlorites, Fe/Mg smectites and prehnite as the result of sub-surface alteration, whereas Al-phyllosilicates as the result of near-surface fluid activity. All the mineralogical features described were interpreted to be related to processes within the craters. This study offers important insights on the Martian palaeoclimate and palaeoenvironment evolution.

**Beiranvand et al. (2017)** (this issue) investigates the applications of ASTER to extract geological information for lithological and alteration mineral mapping as a geological tool for field mapping in remote regions or areas with poorly exposed lithologies, such as the Graham Land, Antarctic Peninsula. They establish a remote sensing satellite-based approach based on qualitative image processing procedures (red, green, blue) composites and band ratios and Principal Components Analysis, by applying matched filter processing to the reflective and thermal bands of ASTER to discriminate mineral assemblages and lithological units. This work supports the efficiency of Landsat-8 and ASTER datasets for extrapolating satellite-based imagery from well-mapped areas into regions with limited map coverage.

**Chen (2017)** (this issue) proposes a methodology for exploration of in coal-bed methane reservoirs at large scale by mapping mineral alteration in areas with vegetation extracting information using open file Sentinel-2 data in the Southern Qishui Basin, China. In this study, the feature extraction of iron and clay minerals were the most precise when compared with known reference data. The accuracy of the results in this study was cross-referenced its results with Hyperion data and X-ray diffraction analysis. This research demonstrates the possibilities of

remote sensing techniques as a low-cost and accurate alternative to explore for coal-bed methane reservoirs.

## Acknowledgements

We would like to thank specially to all the authors of the papers submitted to this special issue, as well as the reviewers who generously supported this publication with their professional and insightful advices. We thank IIT Bombay (India) and the Discovery Program of Mineral Resources in CSIRO (Australia) for their support in the process of putting together this Special Issue. The help of graduate students Akarapu Umamahesh, Malcolm Aranha and Bijal Chudasama (CSRE, IIT Bombay) in preparing the figure and table is gratefully acknowledged.

## Appendix A. Supplementary data

Supplementary data to this article can be found online at <https://doi.org/10.1016/j.oregeorev.2018.12.001>.

Alok Porwal<sup>a,c,\*</sup>, Ignacio González-Álvarez<sup>b,c</sup>,

<sup>a</sup> Centre of Studies in Resources Engineering, IIT Bombay, Powai, India

<sup>b</sup> CSIRO, Mineral Resources, Discovery Program, Kensington, Western Australia, Australia

<sup>c</sup> Centre for Exploration Targeting, University of Western Australia, Crawley, Western Australia, Australia

E-mail address: [aporwal@iitb.ac.in](mailto:aporwal@iitb.ac.in) (A. Porwal).

## References

- Aasen, H., Burkart, A., Bolten, A., Bareth, G., 2015. Generating 3D hyperspectral information with lightweight UAV snapshot cameras for vegetation monitoring: from camera calibration to quality assurance. *ISPRS J. Photogramm. Remote Sens.* 108, 245–259.
- Abrams, M., 2000. The advanced spaceborne thermal emission and reflection radiometer (ASTER): data products for the high spatial resolution imager on NASA's Terra platform. *Int. J. Remote Sens.* 21, 847–859.
- Abrams, M., Hook, S.J., 1995. Simulated ASTER data for geologic studies. *IEEE Trans. Geosci. Remote Sens.* 33, 692–699.
- Anand, R.R., 2015. Importance of 3-D regolith-landform control in areas of transported cover: implications for geochemical exploration. *Geochem. Exploration Environ. Anal.* 16, 14–26.
- Anand, R.R., Butt, C.R.M., 2010. A guide for mineral exploration through the regolith in the Yilgarn Craton, Western Australia. *Austr. J. Earth Sci.* 57, 1015–1114.
- Aubrey, A., Cleaves, H.J., Chalmers, J.H., Skelley, A.M., Mathies, R.A., Grunthaner, F.J., Ehrenfreund, P., Bada, J.L., 2006. Sulfate minerals and organic compounds on Mars. *Geology* 34, 357–360.
- Bedini, E., 2009. Mapping lithology of the Sarfartoq carbonatite complex, southern West Greenland, using HyMap imaging spectrometer data. *Remote Sens. Environ.* 113, 1208–1219.
- Beiravand, A.P., Hashim, M., Hong, J.K., Park, Y., 2017. Lithological and alteration mineral mapping in poorly exposed lithologies using Landsat-8 and ASTER satellite data: north-eastern Graham Land, Antarctic Peninsula. *Ore Geol. Rev. Special Issue*.
- Bishop, J.L., Gross, C., Tirsch, D., Tornabene, L.L., Carter, J., Erkeling, G., 2016. Impacts on Mars: Excavation and/or Hydrothermal Alteration. 79th Annual Meeting of the Meteoritical Society.
- Boccaletti, M., Bonini, M., Mazzuoli, R., Abebe, B., Piccardi, L., Tortorici, L., 1998. Quaternary oblique extensional tectonics in the Ethiopian Rift (Horn of Africa). *Tectonophysics* 287, 97–116.
- Burns, R.G., 1970. Mineralogical applications of Crystal field Theory. Cambridge University Press, pp. 224.
- Burns, R.G., 1997. Origin of electronic spectra of minerals in visible to near-infrared region. In: Pieters, C.M., Englert, A.J. (Eds.), *Remote Geochemical Analysis: Elemental and Mineralogical Composition*. Cambridge University Press, pp. 3–27.
- Butt, C.R.M., 2016. The development of regolith exploration geochemistry in the tropics and sub-tropics. *Ore Geol. Rev.* 73, 380–393.
- Carranza, E.J.M., van Ruitenbeek, F.J.A., Hecker, C., van der Meijde, M., van der Meer, F.D., 2008. Knowledge-guided data-driven evidential belief modeling of mineral prospectivity in Cabo de Gata, SE Spain. *Int. J. Appl. Earth Obs. Geoinf.* 10, 374–387.
- Chen, L., 2017. Potential of sentinel-2 data for alteration extraction in coal-bed methane reservoirs. *Ore Geol. Rev.*
- Chen, X., Warner, T.A., Campagna, D.J., 2007. Integrating visible, near-infrared and short wave infrared hyperspectral and multispectral thermal imagery for geologic mapping: simulated data. *Int. J. Remote Sens.* 28, 2415–2430.
- Clark, R.N., 1999. Spectroscopy of rocks and minerals, and principles of spectroscopy. *Man. Remote Sens.* 3 (3–58), 2.
- Colomina, I., Molina, P., 2014. Unmanned aerial systems for photogrammetry and remote sensing: a review. *ISPRS J. Photogramm. Remote Sens.* 92, 79–97.
- Colwell, R.N., 1983. Manual of remote sensing. Am. Soc. Photogramm. 2440.
- Conte, P., Girelli, V.A., Mandanici, E., 2018. Structure from Motion for aerial thermal imagery at city scale: pre-processing, camera calibration, accuracy assessment. *ISPRS J. Photogramm. Remote Sens.* 146, 320–333.
- Cooper, B.L., Salisbury, W., Killen, R.M., Potter, A.E., 2002. Mid-infrared spectral features of rocks and their powders. *J. Geophys. Res.-Planets* 107.
- Crosta, A.P., Sabine, C., Taranik, J.V., 1998. Hydrothermal alteration mapping at Bodie, California, using AVIRIS hyperspectral data. *Remote Sens. Environ.* 65, 309–319.
- Cudahy, T.J., Rodger, A.P., Barry, P.S., Mason, P., Quigley, M., Folkman, M., & Pearlman, J. (2002, June). Assessment of the stability of the Hyperion SWIR module for hyperspectral mineral mapping using multi-date images from Mount Fitton, Australia. In *Geoscience and Remote Sensing Symposium, 2002. IGARSS'02. 2002 IEEE International* 6, 3504–3506.
- Ehlmann, B.L., Mustard, J.F., Swazey, G.A., Clark, R.N., Bishop, J.L., Poulet, F., Marais, D.J.D., Roach, L.H., Milliken, R.E., Wray, J.J., Barnouin-JHA, O., Murchie, S.L., 2009. Identification of hydrated silicate minerals on Mars using MRO-CRISM: geologic context near Nili Fossae and implications for aqueous alteration. *J. Geophys. Res.-Planets* 114.
- Elachi, C., Zyl, J.V., 2006. *Introduction to the physics and techniques of remote sensing*. John Wiley & Sons.
- Fraser, A., Huggins, P., Rees, J., Cleverly, P., 1997. A satellite remote sensing technique for geological structure horizon mapping. *Int. J. Remote Sens.* 18, 1607–1615.
- Gad, S., Kusky, T., 2006. Lithological mapping in the Eastern Desert of Egypt, the Barramiya area, using Landsat thematic mapper (TM). *J. Afr. Earth Sci.* 44, 196–202.
- Gaffey, S.J., McFadden, L.A., Nash, D., Pieters, C.M., 1997. Ultraviolet, Visible, and Near Infrared Reflectance Spectroscopy: Laboratory Spectra of Geologic Material. In: Pieters, C.M., Englert, A.J. (Eds.), *Remote Geochemical Analysis: Elemental and Mineralogical Composition*. Cambridge University Press, pp. 43–77.
- Gersman, R., Ben-Dor, E., Beyth, M., Avigad, D., Abraha, M., Kibreab, A., 2008. Mapping of hydrothermally altered rocks by the EO-1 Hyperion sensor, Northern Danakil Depression, Eritrea. *Int. J. Remote Sens.* 29, 3911–3936.
- Goetz, A.F.H., Kindel, B., 1996. Understanding unmixed AVIRIS images in Cuprite, NV using coincident HYDICE data". Proc. 6th JPL Air-borne Earth Science Workshop, Pasadena, CA, pp. 96–104.
- Goetz, A.F., Vane, G., Solomon, J.E., Rock, B.N., 1985. Imaging spectrometry for earth remote sensing. *Science* 228 (4704), 1147–1153.
- Gomez, C., Delacourt, C., Allemand, P., Ledru, P., Wackerle, R., 2005. Using ASTER remote sensing data set for geological mapping, in Namibia. *Phys. Chem. Earth* 30, 97–108.
- González-Álvarez, I., Boni, M., Anand, R.R., 2016. Mineral Exploration in Regolith-Dominated Terrains. Global considerations and challenges. *Ore Geol. Rev.* 73, 375–379.
- Hapke, B., 1993. *Theory of Reflectance and Emittance Spectroscopy*. Cambridge University Press, pp. 455.
- Hellman, M.J., Ramsey, M.S., 2004. Analysis of hot springs and associated deposits in Yellowstone National Park using ASTER and AVIRIS remote sensing. *J. Volcanol. Geoth. Res.* 135, 195–219.
- Hewson, R.D., Cudahy, T.J., Mizuhiko, S., Ueda, K., Mauger, A.J., 2005. Seamless geological map generation using ASTER in the Broken Hill-Curnamona province of Australia. *Remote Sens. Environ.* 99, 159–172.
- Hubbard, B.E., Crowley, J.K., Zimbelman, D.R., 2003. Comparative alteration mineral mapping using visible to shortwave infrared (0.4–2.4  $\mu$ m) Hyperion, ALI, and ASTER imagery. *IEEE Trans. Geosci. Remote Sens.* 41, 1401–1410.
- Hunt, G.R., Salisbury, J.W., 1974. Mid-infrared spectral behaviour of igneous rocks. AFCLR-TR-74-0625. Air Force Cambridge Research Laboratories, Hanscom AFB, Massachusetts.
- Hunt, G.R., 1977. Spectral signatures of particulate minerals in the visible and near infrared. *Geophysics* 42 (3), 501–513.
- Hunt, G.R., 1980. Electromagnetic radiation: The communication link in remote sensing. In: Siegel, B.S., Gillespie, A.R. (Eds.), *Remote Sensing in Geology*. Wiley, New York, pp. 5–45.
- Kahle, A.B., Palluconi, F.D., Christensen, P.R., 1997. *Thermal Emission Spectroscopy: Application to Earth and Mars*. In: Pieters, C.M., Englert, A.J. (Eds.), *Remote Geochemical Analysis: Elemental and Mineralogical Composition*. Cambridge University Press, pp. 99–120.
- Kavak, K.S., 2005. Recognition of gypsum geohorizons in the Sivas Basin (Turkey) using ASTER and Landsat ETM+ images. *Int. J. Remote Sens.* 26, 4583–4596.
- Khan, S.D., Mahmood, K., Casey, J.F., 2007. Mapping of Muslim Bagh ophiolite complex (Pakistan) using new remote sensing, and field data. *J. Asian Earth Sci.* 30, 333–343.
- Kratt, C., Calvin, W.M., Coolbaugh, M.F., 2010. Mineral mapping in the Pyramid Lake basin: hydrothermal alteration, chemical precipitates and geothermal energy potential. *Remote Sens. Environ.* 114, 2297–2304.
- Kruse, F.A., 1988. Use of airborne imaging spectrometer data to map minerals associated with hydrothermally altered rocks in the Northern Grapevine Mountains, Nevada and California. *Remote Sens. Environ.* 24 (1), 31–51.
- Kruse, F.A., 2008. Expert System Analysis of Hyperspectral Data, Algorithms and Technologies for Multispectral, Hyperspectral, and Ultraspectral Imagery XIV. Proc. SPIE 6966, 1–12.

\* Corresponding author.

- Kruse, F.A., 2012. Mapping surface mineralogy using imaging spectrometry. *Geomorphology* 137, 41–56.
- Kruse, F. A., 2015. Comparative analysis of airborne visible/infrared imaging spectrometer (AVIRIS), and hyperspectral thermal emission spectrometer (HyTES) longwave infrared (LWIR) hyperspectral data for geologic mapping. In: Algorithms and Technologies for Multispectral, Hyperspectral, and Ultraspectral Imagery XXI (Vol. 9472, p. 94721F). International Society for Optics and Photonics.
- Kruse, F.A., Kierein-Young, K.S., Boardman, J.W., 1990. Mineral mapping at Cuprite, Nevada with a 63 channel imaging spectrometer. *Photogramm. Eng. Remote Sens.* 56 (1), 83–92.
- Kruse, F.A., Lefkoff, A.B., Dietz, J.B., 1993. Expert system-based mineral mapping in northern Death Valley, California/Nevada, using the airborne visible/infrared imaging spectrometer (AVIRIS). *Remote Sens. Environ.* 44 (2–3), 309–336.
- Kruse, F.A., Boardman, J.W., Huntington, J.F., 1999. Fifteen years of hyperspectral data: Northern Grapevine Mountains, Nevada. Proc. 8th JPL Airborne Earth Science Workshop, Pasadena, CA, pp. 47–258.
- Kruse, F.A., Boardman, J.W., Huntington, J.F., 2003. Comparison of airborne hyperspectral data and EO-1 hyperion for mineral mapping. *IEEE Trans. Geosci. Remote Sens.* v. 41(6).
- Kruse, F.A., Perry, S.L., Caballero, A., 2006. District-level mineral survey using airborne hyperspectral data, Los Menudos, Argentina. *Ann. Geophys.* 49, 83–92.
- Kumar, V.K., Porwal, A., Rani, K., Sahoo, K., Singaravelu, V., Singh, R.P., Khandelwal, M.K., Kumar, A., Raju, P.V., Diwakar, P.G., 2018. Reflectance spectroscopy and ASTER based mapping of rock-phosphate in parts of Paleoproterozoic sequences of Aravalli Group of rocks, Rajasthan, India. *Ore Geol. Rev.*
- Lafuente, B., Downs, R.T., Yang, H., Stone, N., 2015. The power of databases: the RRUFF project. In: Armbruster, T., Danisi, R.M. (Eds.), *Highlights in Mineralogical Crystallography*. Berlin, Germany, W. De Gruyter, pp. 1–30.
- Lampinen, H., Laukamp, C., Oechcipinti, S., Metelka, V., Spinks, S., 2017. Delineating alteration footprints from field and ASTER SWIR spectra, geochemistry and gamma-ray spectrometry above regolith-covered base metal deposits – an example from Abra, Western Australia. *Econ. Geol.* 112, 1977–2003.
- Li, P.J., Long, X.Y., Liu, L., 2007. Ophiolite mapping using ASTER data: a case study of Derni ophiolite complex. *Acta Petrologica Sinica* 23, 1175–1180.
- Loizeau, D., Mangold, N., Poulet, F., Bibring, J.P., Gendrin, A., Ansan, V., Gomez, C., Gondet, B., Langevin, Y., Masson, P., Neukum, G., 2007. Phyllosilicates in the Mawrth Vallis region of Mars. *J. Geophys. Res.-Planets* 112.
- Macdonald, I.R., Guinasso, N.L., Ackleson, S.G., Amos, J.F., Duckworth, R., Sassen, R., Brooks, J.M., 1993. Natural oil-slicks in the Gulf-of-Mexico visible from space. *J. Geophys. Res.-Oceans* 98, 16351–16364.
- Madani, A.A., Emam, A.A., 2011. SWIR ASTER band ratios for lithological mapping and mineral exploration: a case study from El Hudi area, southeastern desert, Egypt. *Ar. J. Geosci.* 4, 45–52.
- Mangold, N., Gendrin, A., Gondet, B., Lemouelic, S., Quantin, C., Ansan, V., Bibring, J.P., Langevin, Y., Masson, P., Neukum, G., 2008. Spectral and geological study of the sulfate-rich region of West Candor Chasma, Mars. *Icarus* 194, 519–543.
- Mars, J.C., Rowan, L.C., 2006. Regional mapping of phyllitic- and argillitic-altered rocks in the Zagros magmatic arc, Iran, using Advanced Spaceborne Thermal Emission and Reflection Radiometer (ASTER) data and logical operator algorithms. *Geosphere* 2, 161–186.
- Mars, J.C., Rowan, L.C., 2010. Spectral assessment of new ASTER SWIR surface reflectance data products for spectroscopic mapping of rocks and minerals. *Remote Sens. Environ.* 114, 2011–2025.
- Mars, J.C., Rowan, L.C., 2011. ASTER spectral analysis and lithologic mapping of the Khanneshin carbonatite volcano, Afghanistan. *Geosphere* 7, 276–289.
- Massironi, M., Bertoldi, L., Calafa, P., Visona, D., Bistacchi, A., Giardino, C., Schiavo, A., 2008. Interpretation and processing of ASTER data for geological mapping and granitoids detection in the Saghro massif (eastern Anti-Atlas, Morocco). *Geosphere* 4, 736–759.
- Mustard, J.F., Murchie, S.L., Pelkey, S.M., Ehlmann, B.L., Milliken, R.E., Grant, J.A., Bibring, J.P., Poulet, F., Bishop, J., Dobrea, E.N., Roach, L., Seelos, F., Arvidson, R.E., Wiseman, S., Green, R., Hash, C., Humm, D., Malaret, E., McGovern, J.A., Seelos, K., Clancy, T., Clark Des Marais, R., Izenberg, D., Knudson, N., Langevin, A., Martin, Y., McGuire, T., Morris, P., Robinson, R., Roush, M., Smith, T., Swazey, M., Taylor, G., Titus, H., Wolff, T.M., 2008. Hydrated silicate minerals on Mars observed by the Mars Reconnaissance Orbiter CRISM instrument. *Nature* 454, 305–309.
- Ninomiya, Y., Fu, B., 2018. Thermal infrared multispectral remote sensing of lithology and mineralogy based on spectral properties of materials. *Ore Geol. Rev.*
- Oztan, N.S., Suzen, M.L., 2011. Mapping evaporate minerals by ASTER. *Int. J. Remote Sens.* 32, 1651–1673.
- Pajares, G., 2015. Overview and current status of remote sensing applications based on unmanned aerial vehicles (UAVs). *Photogramm. Eng. Remote Sens.* 81 (4), 281–330.
- Pearlman, J.S., Barry, P.S., Segal, C.C., Shepanski, J., Beiso, D., Carman, S.L., 2003. Hyperion, a space-based imaging spectrometer. *IEEE Transactions on Geoscience and Remote Sensing*, pp. 1160–1173.
- Qari, M.H.T., Madani, A.A., Matsah, M.I.M., Hamimi, Z., 2008. Utilization of ASTER and Landsat data in geologic mapping of basement rocks of Arafat Area, Saudi Arabia. *Ar. J. Sci. Eng.* 33, 99–116.
- Rockwell, B.W., Hofstra, A.H., 2008. Identification of quartz and carbonate minerals across northern Nevada using ASTER thermal infrared emissivity data—implications for geologic mapping and mineral resource investigations in well-studied and frontier areas. *Geosphere* 4, 218–246.
- Rowan, L.C., Crowley, J.K., Schmidt, R.G., Ager, C.M., Mars, J.C., 2000. Mapping hydrothermally altered rocks by analyzing hyperspectral image (AVLIRIS) data of forested areas in the Southeastern United States. *J. Geochem. Explor.* 68, 145–166.
- Rowan, L.C., Mars, J.C., 2003. Lithologic mapping in the Mountain Pass, California area using advanced spaceborne thermal emission and reflection radiometer (ASTER) data. *Remote Sens. Environ.* 84, 350–366.
- Salisbury, J.W., 1997. Mid-infrared Spectroscopy: Laboratory Data. In: Pieters, C.M., Englert, A.J. (Eds.), *Remote Geochemical Analysis: Elemental and Mineralogical Composition*. Cambridge University Press, pp. 79–99.
- Sankaran, R., Nasir, S., this issue. Application of ASTER data to mineral targeting in arid regions with special reference to Oman: A review. *Ore Geology Reviews Special Issue*.
- Schetselaar, E.M., Chung, C.J.F., Kim, K.E., 2000. Integration of Landsat TM, gamma ray, magnetic, and field data to discriminate lithological units in vegetated granite-gneiss terrain. *Remote Sens. Environ.* 71, 89–110.
- Shevrev, S., 2018. Neotectonics, remote sensing and erosion cut of ore-controlling structures of the Mnogovershinnoe gold-silver deposit (Khabarovsk Krai, Russian Far East). *Ore Geol. Rev.*
- Singh, P., Sarkar, R., Porwal, A., 2017. Orbital remote sensing of impact-induced hydrothermal systems on Mars. *Ore Geol. Rev.*
- Sledz, A., Unger, J., Heipke, C., Thermal, I.R., 2018. Imaging: image quality and orthophoto generation. *Int. Arch. Photogramm., Remote Sens. Spatial Inf. Sci.* 42 (1).
- Tayara, H., Chong, K., 2018. Object detection in very high-resolution aerial images using one-stage densely connected feature pyramid network. *Sensors* 18 (10), 3341.
- Turner, D., Lucieer, A., Wallace, L., 2014. Direct georeferencing of ultrahigh-resolution UAV imagery. *IEEE Trans. Geosci. Remote Sens.* 52 (5), 2738–2745.
- Van der Meer, F.D., 2006. The effectiveness of spectral similarity measures for the analysis of hyperspectral imagery. *Int. J. Appl. Earth Obs. Geoinf.* 8, 3–17.
- Van der Meer, F.D., van Dijk, P., van der Werff, H., Yang, H., 2002. Remote sensing and petroleum seepage: a review and case study. *Terra Nova* 14, 1–17.
- Van der Meer, F.D., van der Werff, H.M., van Ruitenberg, F.J., Hecker, C.A., Bakker, W.H., Noomen, M.F., van der Meijde, M., Carranza, E.J.M., de Smeth, J.B., Wol dai, T., 2012. Multi-and hyperspectral geologic remote sensing: a review. *Int. J. Appl. Earth Obs. Geoinf.* 14 (1), 112–128.
- Vasuki, Y., Yu, L., Holden, E.-J., Kovesi, P., Wedge, D., Grigg, A., 2018. The spatial-temporal patterns of land cover changes due to mining activities in the Darling Range, Western Australia: a visual analytics approach. *Ore Geol. Rev.*
- Vaughan, R.G., Hook, S.J., Calvin, W.M., Taranik, J.V., 2005. Surface mineral mapping at Steamboat Springs, Nevada, USA, with multi-wavelength thermal infrared images. *Remote Sens. Environ.* 99, 140–158.
- Vickers, R.S., Lyon, R.J.P., 1967. Infrared sensing from space-craft: A geological interpretation. In: Heller, O.B. (Ed.), *Thermophysics of Space Craft and Planetary Bodies – Properties of Solids and the Electromagnetic Radiation*. Academic, New York, pp. 70–79.
- Vincent, R.K., Thomson, F., 1972. Spectral compositional imaging of silicate rocks. *J. Geophys. Res.* 77 (1972), 2465–2471.
- Wang, A., Freeman, J.J., Jolliff, B.L., Chou, I.M., 2006. Sulfates on Mars: a systematic Raman spectroscopic study of hydration states of magnesium sulfates. *Geochim. Cosmochim. Acta* 70, 6118–6135.
- Watts, D.R., Harris, N.B.W., Grp, N.G.S.W., 2005. Mapping granite and gneiss in domes along the North Himalayan antiform with ASTER SWIR band ratios. *Geol. Soc. Am. Bull.* 117, 879–886.
- Yamaguchi, Y., Kahle, A.B., Tsu, H., Kawakami, T., Pniel, M., 1998. Overview of advanced spaceborne thermal emission and reflection radiometer (ASTER). *IEEE Trans. Geosci. Remote Sens.* 36, 1062–1071.
- Yamaguchi, Y., Naito, C., 2003. Spectral indices for lithologic discrimination and mapping by using the ASTER SWIR bands. *Int. J. Remote Sens.* 24, 4311–4323.
- Yang, K., Browne, P.R.L., Huntington, J.F., Walshe, J.L., 2001. Characterising the hydrothermal alteration of the Broadlands-Ohaaki geothermal system, New Zealand, using short-wave infrared spectroscopy. *J. Volcanol. Geoth. Res.* 106, 53–65.
- Yang, K., Huntington, J.F., Browne, P.R.L., Ma, C., 2000. An infrared spectral reflectance study of hydrothermal alteration minerals from the Te Mihi sector of the Wairakei geothermal system, New Zealand. *Geothermics* 29, 377–392.
- Yesou, H., Besnus, Y., Rolet, J., 1993. Extraction of spectral information from Landsat TM data and merger with SPOT panchromatic imagery – a contribution to the study of geological structures. *ISPRS J. Photogramm. Remote Sens.* 48, 23–36.
- Zhang, X., Pamer, M., Duke, N., 2007. Lithologic and mineral information extraction for gold exploration using ASTER data in the south Chocolate Mountains (California). *ISPRS J. Photogramm. Remote Sens.* 62, 271–282.
- Zhao, B., Yang, F., Pilz, J., Zhang, D., 2018. A novel approach for extraction of Gaoshanhe-Group outcrops using Landsat Operational Land Imager (OLI) data in the heavily loess-covered Baoji District, Western China. *Ore Geol. Rev.*